ACS central science

Research Article

http://pubs.acs.org/journal/acscii

Self-Assembled Multifunctional Hybrids: Toward Developing High-Performance Graphene-Based Architectures for Energy Storage Devices

Md. Monirul Islam, Seyed Hamed Aboutalebi, Dean Cardillo, Hua Kun Liu, Konstantin Konstantinov,* and Shi Xue Dou

Institute for Superconducting and Electronic Materials, Australian Institute for Innovative Materials (AIIM) Facility, University of Wollongong, Innovation Campus, North Wollongong, New South Wales 2522, Australia

Supporting Information

ABSTRACT: The prospect of developing multifunctional flexible three-dimensional (3D) architectures based on integrative chemistry for lightweight, foldable, yet robust, electronic components that can turn the many promises of graphene-based devices into reality is an exciting direction that has yet to be explored. Herein, inspired by nature, we demonstrate that through a simple, yet novel solvophobic self-assembly processing approach, nacre-mimicking, layer-by-layer grown, hybrid composite materials (consisting of graphene oxide, carbon nanotubes, and conducting polymers) can be made that can incorporate many of the exciting attributes of graphene into real world materials. The as-produced, self-assembled 3D multifunctional architectures were found to be flexible, yet mechanically robust and tough (Young's modulus in excess of 26.1 GPa, tensile strength of around 252 MPa, and toughness of 7.3 MJ m^{-3}), and exhibited high native electrical conductivity (38700 S m^{-1}) and unrivalled volumetric capacitance values (761 F cm^{-3}) with excellent cyclability and rate performance.

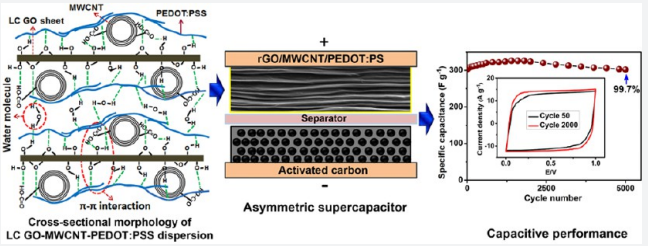

INTRODUCTION

Recent developments on single-component carbon nanomaterials, such as one-dimensional (1D) carbon nanotubes (CNTs)[1,2] and two-dimensional (2D) graphene,[3] have paved the way to using these interesting materials in a broad range of devices and applications, ranging from biomedical implants[2,4,5] to more sophisticated applications such as the energy-storage systems[6−13] needed to power up flexible, smart wearable garments[11,13−15] and miniaturized electronic gadgets.[16−18] The strong direction-dependent properties of these materials, however, resulting from their very weak out-of-plane transport properties have necessitated exploring ways to extend their properties into the third dimension.[7−9,19−22] Addressing this challenge is, therefore, crucial to realize the hybrid high-performance multifunctional architectures required for numerous applications, including, but not limited to, energy-storage devices, integrated micro- and nano-electromechanical systems, and implantable biomedical devices.

The integration of multicomponent carbon-based materials has been utilized to address such challenges to some extent. The most prominent example is the use of carbon nanotubes as spacers between graphene sheets to prevent them from restacking.[7,9,13,21−24] Such a three-dimensional (3D) network architecture can, in principle, promote the simultaneous enhancement of both mechanical properties[22] and transport properties,[20,21] although achieving these sorts of structures, in practice and not only in theory, with precise control over their functional domains is a challenging, if not impossible, task. We have previously demonstrated that, through simple control of the solvophobic self-assembly interactions inherent in liquid crystalline dispersions of ultralarge graphene oxide sheets,[22,25] such levels of control can be exercised to fabricate graphene-based hybrid composites with carbon nanotubes (CNTs),[7,9] metal-based compounds,[26−28] and polymers,[29] leading to building blocks for cost-effective, high-capacity supercapacitor electrodes and hydrogen storage media. This suggests that, with further improvements, these types of composites could play a leading role in addressing one of the main sticking points for extending the intriguing properties of single-component carbon nanomaterials into multicomponent multidimensional 3D frameworks: a simple nanofabrication approach to the design of chemically and spatially tunable hybrid architectures for use as multifunctional architectures for a wide range of applications.

In the present work, we demonstrate a simple, straightforward, liquid crystal mediated self-assembly approach based on the interfacial coupling of liquid crystalline graphene oxide (LC GO), multiwalled CNTs (MWCNTs), and an amphiphilic conducting polymer (CP) [poly(3,4-ethylenedioxythiophene):poly(styrenesulfonate) (PEDOT:PSS)] to fabricate unlimited lengths of multicomponent 3D network architectures. The as-produced architectures

Received: February 18, 2015
Published: July 2, 2015

DOI: 10.1021/acscentsci.5b00189
ACS Cent. Sci. 2015, 1, 206−216

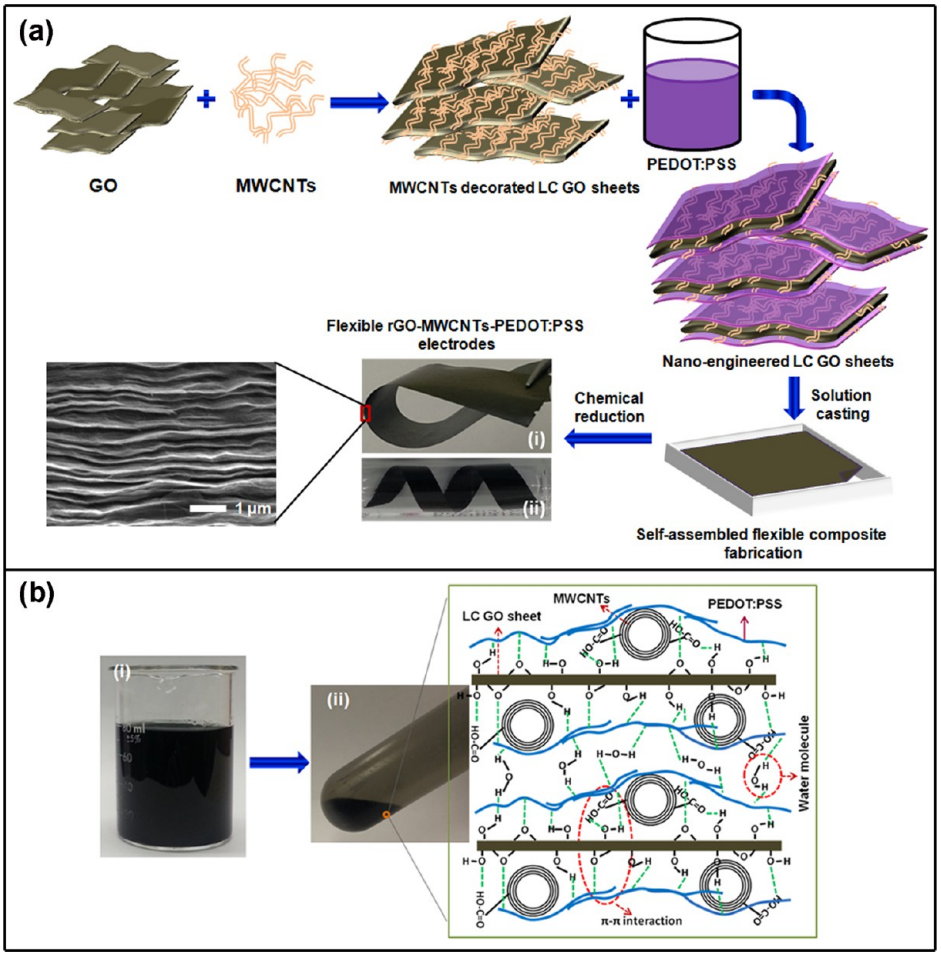

Figure 1. Graphical illustration of the self-assembly process. (a) Interaction of MWCNTs and PEDOT:PSS on ultralarge LC GO sheets, resulting in self-assembled layer-by-layer flexible electrodes. (b) Incubated dispersion of LC GO-MWCNT-PEDOT:PSS (i), and dispersion after centrifuging to decant the excess PEDOT:PSS to obtain the required composite dispersion (ii). Inset shows the proposed cross-sectional morphology of a multifunctional domain comprising MWCNTs and PEDOT:PSS stabilized on liquid crystalline graphene oxide sheets through $\pi-\pi$ interaction and hydrogen bonding.

exhibited unrivalled collective electrical, electrochemical, and mechanical properties, making them suitable building blocks to answer the immediate need for multifunctional architectures with superior properties for flexible integrated devices. The simple fabrication of this flexible hybrid composite results in an advanced interconnecting conductive network with favorable electrochemical performance and has great potential to be scaled up for large-scale energy storage device electrode preparation.

RESULTS AND DISCUSSION

Fabrication of Self-Assembled Flexible Ternary Composite. Among many self-assembling systems, by the virtue of their very own nature (their mobility at the molecular level while exhibiting their liquid crystalline (LC) state order at the same time), large mesogens are envisaged as unique primary candidates for matrix-guided molecular level self-assembly of nanomaterials.[9,22,30−33] This, in practice, means that the programming of rich, architecturally diverse, and complex structures through controlled decoration of liquid crystal mesogens with different materials in the solution phase is possible. Inspired by this idea, LC GO-CNT based composite formulations were introduced with interesting mechanical and energy storage properties,[7,9,22] although such formulations have been limited to the chemistry of graphene oxide (i.e., they do not make use of the hydrophilic regions on graphene oxide, essentially leading to modest conductivities and electrochemical activities). Amphiphilic conducting polymers, such as PEDOT:PSS, however, can contribute to higher capacitance values by tapping into Faraday redox reactions. Moreover, if combined with hybrid LC GO-CNT formulations, they can occupy the vacant space on GO sheets while not disturbing the stability of the mesogens and forming aggregates, as the components are both physically and chemically joined (Figure 1). In addition, the flexibility of PEDOT:PSS makes it a very good geometrical fit, as it can easily wrap the entire architecture and impose selectivity on the resulting interactions. By controlling the ratio with respect to the initially decorated MWCNTs, it is then possible to influence the content of naturally anchored PEDOT:PSS on the LC GO sheet surface as a secondary material. We utilized LC GO to induce liquid crystallinity in the CNT and conductive polymer (CP) dispersion through the addition of LC GO to the CNT and CP dispersion. The superior amphiphilicity of ultralarge LC GO sheets not only facilitates the instantaneous surface assembly on the nanoscale of two different conductive materials but also allows the entire architecture to remain stable in the liquid crystalline state. A graphical depiction of the processing is provided in Figure 1.

DOI: 10.1021/acscentsci.5b00189
ACS Cent. Sci. 2015, 1, 206−216

Representative cross-polarized optical microscope (POM) micrographs of the GCNTPP dispersion in Figure 2 clearly

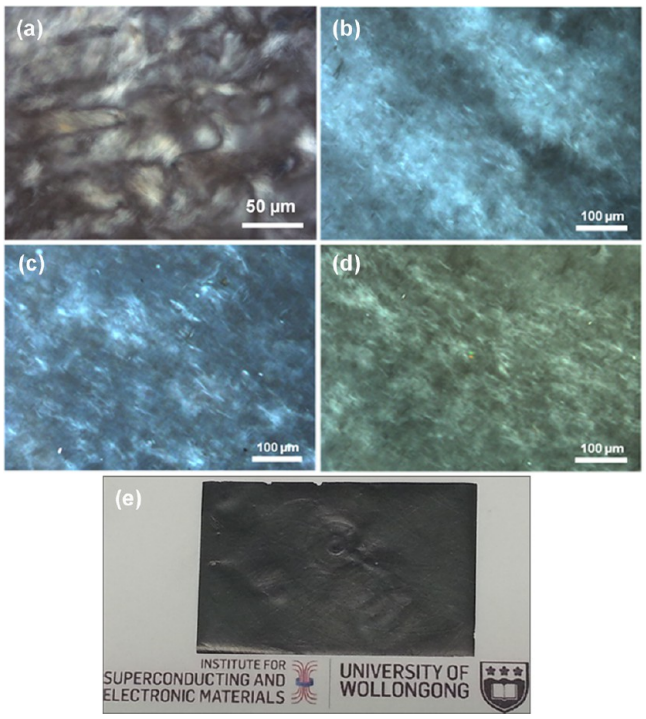

Figure 2. Representative cross-polarized optical microscope images. (a) Aqueous LC GO shows a typical schlieren texture at a concentration of 2.5 mg mL^{-1}. Even with the addition of varying amounts of MWCNTs and PEDOT:PSS to form (b) GCNTPP 5, (c) GNCTPP 10, and (d) GCNTPP 15, the structure still shows the typical optical behavior of liquid crystals at 5 mg mL^{-1} of composite dispersions, suggesting that the addition of both CNTs and the polymer could not disturb the LC behavior. The as-prepared hybrid LC was then cast to achieve (e) a nacre-mimicking free-standing film (12 × 8 cm^2 in size).

show the birefringence typical of lyotropic nematic liquid crystals, which is similar to that of bare LC GO. Large areas of uniform orientation with occasional defects were observed, indicating the full orientation of large mesogenic domains. The existence of such large mesogenic domains therefore facilitates the processing and casting of the final composition in basically unlimited sizes, which is crucial for any real-world application of these materials.

Materials Analysis of the Layer-by-Layer Ternary Composite. To observe the geometrical effects of the low-temperature chemical reduction route on the self-assembled 3D architectures and GO sheet morphology, cross-sectional FE-SEM and HRTEM microscopy were performed on the as-reduced architectures (Figure 3). Cross-sectional FE-SEM images clearly showed no visible swelling after reduction, which is typical of hydrazine treated architectures and indicative of uniform and homogeneous reduction of the final architecture. Furthermore, the electron microscope images demonstrate that the interacting MWCNTs and PEDOT:PSS are homogeneously distributed both on the surface of the rGO sheets and also between the sheets, bridging them together (Figure 3) and thus creating a highly conductive 3D network architecture. Moreover, the introduction of such ternary architectures leads to increased broad *d*-spacing and pore sizes in the final architecture, ranging from 5.4 to 8.6 Å (as evidenced by the XRD patterns presented in the Supporting Information, Figure S6). Such an expansion in the distance between the neighboring layers can improve the accessibility of interlayer spacing, as it is on the order of the charge separation, suggesting the possibility of the complete use of electric double layer capacitance within the system in conjunction with pseudocapacitance.[11]

All hybrid composites fabricated by the method described here demonstrated exceptional conductivity, with the best of them exhibiting a native conductivity of ~38700 ± 7987 S m^{-1} (Table S1), which is 2 orders and 1 order of magnitude higher than for previously reported PEDOT:PSS paper (100 S m^{-1}), our previous report on LC GO/SWCNT hybrids (1500 S m^{-1}), and rGO paper (3280 S m^{-1}), respectively. It is also even much higher than for polyaniline (PANI) reinforced graphene nanoribbon-CNT hybrids (18000 S m^{-1}), MWCNT reinforced PANI (33100 S m^{-1}), different types of bucky papers (22000 S m^{-1}), and the best of the rGO-CNT papers (36000 S m^{-1}). This can be explained by the high alignment of rGO sheets, the individual dispersion of MWCNTs, and the complete wrapping of both rGO and MWCNTs by PEDOT:PSS in the final architecture. Additionally, ascorbic acid during the redox reaction[34] and sulfuric acid at room temperature[35] play a very important role in the transformation of the benzoid structure of the PEDOT backbone to the quinoid structure to experience excellent electrical conductivity. For MWCNT content higher than 10 wt %, however, some occasional aggregation and agglomeration of MWCNTs can be observed (Figure 3c) which interrupt the $\pi-\pi$ interaction of PEDOT:PSS on the GO surface, interfering with the conductive polymer layer; it decreases the conductivity of rGCNTPP composite. Moreover these levels of agglomeration, although they cannot disturb the stability of the LC dispersion, can have a detrimental effect on the conductivity, as the interlocking of MWCNTs within the structure increases the overall resistivity of the materials. Due to this effect, the conductivity of rGCNTPP 15 decreases to ~26900 ± 5631 S m^{-1} (Table S1). MWCNTs, as very strong direction-dependent conductors, are known to conduct electricity through their length, and as such, they are unable to afford out-of-plane electron conduction. Therefore, any interlocking and agglomeration of MWCNTs at an angle to their length can effectively only result in an increase in resistivity. It was therefore found that there is an optimum ratio of PEDOT:PSS to MWCNTs resulting from the interplay among all three materials that allows for higher conductivity. [See the Supporting Information for the structural and quantitative analysis of the as-prepared rGCNTPP composites as well as their thermal and mechanical performance. FT-IR (Figure S2) and UV−vis (Figure S3) analyses were carried out to demonstrate the stability of the PEDOT:PSS during the reduction process. The EDS (Figure S4, Table S2) and XPS (Figure S5, Table S3) analyses were conducted to optimize the quantity of $\pi-\pi$ interacting PEDOT:PSS, and Table S4 represents the composition of the final composites. Moreover, XRD (Figure S6), BET (Figure S7 and Table S5), TGA (Figure S8), and mechanical performance (Figure S9, Table S6) analyses were carried out to explore and explain the interlayer spacing of the layer-by-layer architecture, the generated specific surface area, the quantitative thermal stability of the components, and the mechanical stability of the 3D architectures, respectively.]

Such attributes also manifested themselves in the mechanical properties measured for our as-prepared architectures (Figure

DOI: 10.1021/acscentsci.5b00189
ACS Cent. Sci. 2015, 1, 206−216

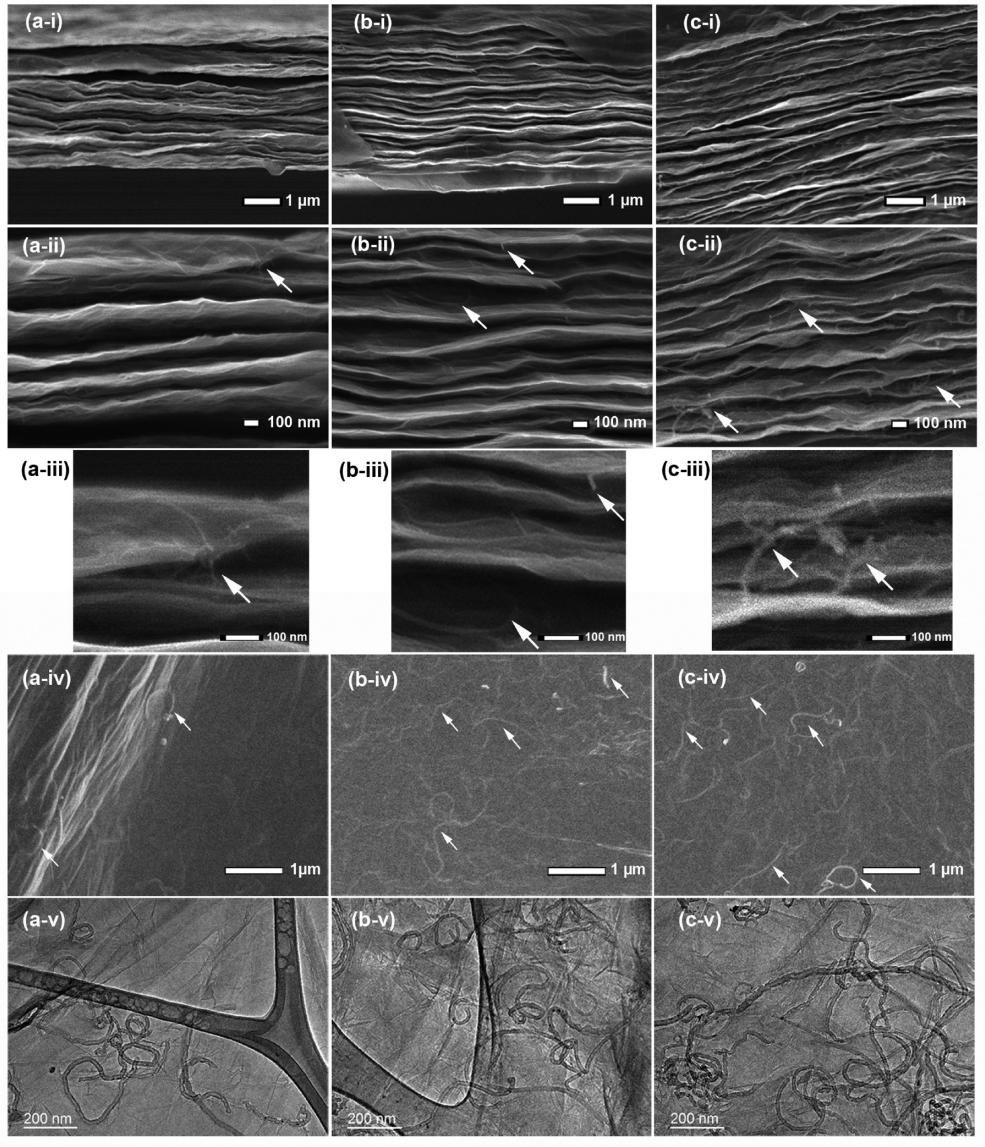

Figure 3. Electron microscope images of the as-prepared hybrid architectures. Cross-sectional FE-SEM images of the rGCNTPP composites in low and high magnification (rows i and ii, respectively): (a) rGCNTPP 5, (b) rGCNTPP 10, and (c) rGCNTPP15, showing how the interlayer structure of the composites is influenced by the various amounts of MWCNTs (marked with arrows in row ii and magnified images in row iii) and the natural assembly of covalently interacted PEDOT:PSS. The surface morphology of the composites obtained by FE-SEM (row iv, arrows indicate the MWCNTs) and HRTEM images (row v) of the corresponding as-prepared composites reveals the architecture of the MWCNT/PEDOT:PSS interacting with rGO sheets.

S9, Table S6). The best graphene-based hybrid composite's Young's modulus (~29.2 GPa) outperformed those of all other previously reported GO and rGO based fibers, and was found to be even higher than for our previously reported cross-linked GO and rGO-based fibers, such as GO fibers coagulated in chitosan (~22.6 GPa) and $CaCl_2$ (~20.1 GPa), and pure GO fibers coagulated in acetone (~20.5 GPa).[11,36−38] Our average Young's modulus is also considerably higher than those reported for bucky papers,[39] paperlike materials based on vermiculite,[40] flexible graphite foil,[41,42] and layer-by-layer assembled MWCNT nanocomposites,[43] and just inferior to our previously reported SWCNT/rGO hybrids.[22] This represents a massive impact generated by the natural interaction between graphene oxide sheets with MWCNTs and further $\pi-\pi$ interaction of PEDOT:PSS with the remaining functional groups of graphene oxide. The strong $\pi-\pi$ interaction between GO and PEDOT:PSS makes the π-electron system of PEDOT:PSS more stable,[44] keeps the polymer backbone smooth, and provides overall stability to the polymer layer on the graphene oxide surface. It helps the rGCNTPP composite to become more flexible than rGO film. Above all, the homogeneously decorated interlayer MWCNTs act as a very strong flexible support for the layer-by-layer structure. All these synergistic effects give this rGCNTPP ternary composite a mechanically robust structure. The higher degree of hydrogen bonding within the structure, due to the acidic condition in which the reduction process was performed, results in stronger interactions between rGO sheets. Moreover, the presence of PEDOT:PSS contributes to more adsorption of moisture from ambient atmosphere resulting in more pronounced hydrogen bonding and higher levels of stiffness and toughness. This is a byproduct of the highly charged

DOI: 10.1021/acscentsci.5b00189
ACS Cent. Sci. 2015, 1, 206−216

Table 1. Specific Capacitance of As-Prepared rGCNTPP 10 Composite against Previous Reports on Graphene/CNT/Conductive Polymer (CP) Composites in Different Systems

Two-Electrode System							
composite	mass	voltage window (V)	electrolyte	specific capacitance (F g^{-1})	energy density (Wh kg^{-1})	power density (kW kg^{-1})	ref
rGCNTPP 10 (solution cast)	0.95 mg/cm^2	0−1	1 M H_2SO_4	364 @ 5 mV s^{-1}, 318 @ 1 A g^{-1}	11.4	0.145	present work
graphene/CNT/PANI (electropolymerization)	0.4 mg/cm^2	0−1/0−4	1 M KCl	271 @ 0.3 A g^{-1}	188.4	2.7	53
rGO/PVP (drop casting on adhesive tape)		0−1	1.5 M TEA-BF_4	168 @ 1 A g^{-1}			54
PEDOT/A-CNT/graphene (in situ polymerization)		0−4	2 M $BMIBF_4$/propylene	81.6 @ 0.2 A g^{-1}	176.6	233	55
rGO/PPy (in situ polymerization)	1.3 mg/cm^2	0−1.6	1 M Na_2SO_4	248.8	21.4	0.453	56
sGNS/cMWCNT/PANI (in situ polymerization)	1.6 mg/cm^2	0−1.6	1 M H_2SO_4	75 @ 1 A g^{-1}	20.5	25	57
SRGO (thermal treatment)		−0.3−0.3	PVA−H_2SO_4	140 @ 1 A g^{-1}			58
CNT-PPy sponge (Electro polymerization)		−0.45−0.45	2 M KCl	335 @ 2 mV s^{-1}			59
MWCNT-PANI (electropolymerization)	1.41 $\mu g/cm^2$	−0.2−0.8	PVA−H_3PO_4	233 @ 1 A g^{-1}			60
3D RGO/PANI (in situ polymerization)		0−1	1 M H_2SO_4	385 @ 0.5 A g^{-1}			61
MWCNT/PPy/rGO/NWF (in situ polymerization)		−0.5−0.5	1 M KCl	319 @ 1 mV s^{-1}			62
EVPP-PEDOT (vapor phase polymerization)	1 $\mu g/cm^2$	0−1/0−2	6 M KCl/1 M TBAH	175 @ 5 mV s^{-1}	2.4	3.6	52

Three-Electrode System					
composite	mass	voltage window (V)	electrolyte	specific capacitance (F g^{-1})	ref
rGCNTPP 10 (solution cast)	0.95 mg/cm^2	0−0.9	1 M H_2SO_4	657 @ 5 mV s^{-1}	present work
rGO-MWCNTs (solution cast)	1 mg/cm^2	−0.2−0.5	1 M H_2SO_4	251 @ 5 mV s^{-1}	7
GO-PEDOT:PSS-CNT (solution cast)	0.3 mg	−1−1	6 M $NaNO_3$	365 @ 1 mV s^{-1}	63
RGO-PEDOT (in situ polymerization)	2 mg	−0.4−0.6	1 M H_2SO_4	108 @ 0.3 A g^{-1}	64
graphene/PEDOT (microwave-assisted)		−0.2−0.8	1 Ml H_2SO_4	270 @ 1 A g^{-1}	65

Table 2. Volumetric Capacitance of the As-Prepared rGCNTPP 10 Composite in Comparison with Different Carbon-Based Electrode Materials

composite	electrode thickness (μm)	potential window (V)	volumetric capacitance (F cm^{-3})	ref
rGCNTPP 10	8.2	0−1	761 @ 5 mV s^{-1}	present work
titanium carbide	5	−0.3−0.3	910 @ 2 mV s^{-1}	48
compressed a-MEGO	57	0−3.5	110 @ 100 mV s^{-1}	49
VArGO	270	−0.1−0.7	171 @ 0.5 A g^{-1}	50
compact EM-CCG film	25	0−1	261.3 @ 0.1 A g^{-1}	10

surface profile of each layer, contributing to the alignment and structuring of interfacial water and a more highly structured hydrogen bonding network.[45,46] In terms of ultimate stress, our average ultimate stress was also considerably higher than for all those other paper-like architectures and was inferior to that in our previous report on LC GO/SWCNTs[22] and graphene paper prepared by vacuum filtration.[47] Nevertheless, by the measure of overall mechanical performance, the toughness of our as-prepared architectures was found to be higher than for all of the other carbon and polymer-based architectures reported here, due to the very high elongation at breaking of our hybrid composites, which was only lower than for LC GO/SWNTs.[22]

Capacitive Performance of the Free-Standing Ternary Composite Electrode. The high mechanical stability and interesting electrical conductivity of our as-prepared rGCNTPP composites make them potentially highly suitable for a range of different applications, including large-area electronics and structural multifunctional composite applications. Moreover, for application as supercapacitors, the mechanical stability of these materials means that they can be used in the form of paper electrodes that can simultaneously act as both the current collector and the active material. As a proof of concept, we prepared a range of different electrodes and devices to evaluate the capacitance performance of the hybrid architectures, most importantly from the electrochemical performance revealed by their cyclic voltammogram (CV) response at 5 mV s^{-1} (Figure S10). Preliminary electrochemical studies using a three-electrode configuration setup demonstrated the excellent capacitive properties of the self-assembled rGCNTPP composites (see the Supporting Information for the capacitive performance of individual free-standing ternary composite electrodes in three-electrode system). The rGCNTPP 10 composite showed the best performance, with a high specific capacitance of 657 F g^{-1} at 5 mV s^{-1} and 436 F g^{-1} at 100 mV s^{-1}. This is a 10-fold increase as compared to rGO, 7-fold as compared to PEDOT:PSS, and 8-fold as compared to MWCNTs,[7] making it the highest among the GO/CNT/PEDOT:PSS systems (Table 1). Moreover, these additive-free hybrid composites demonstrated volumetric capacitance of up to 761 F cm^{-3} at 5 mV s^{-1}, presenting an almost 3-fold increase over the best volumetric capacitances of carbon-based electro-

DOI: 10.1021/acscentsci.5b00189
ACS Cent. Sci. 2015, 1, 206−216

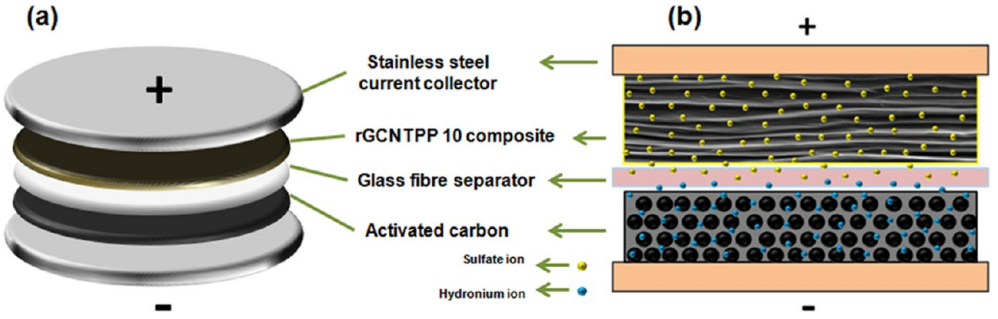

Figure 4. Graphical illustration of asymmetric supercapacitor device assembled in ECC-Std electrochemical test cell with 1 M H_2SO_4 electrolyte (a), and electrochemical interaction of electrolyte ions between the cathode and anode (b).

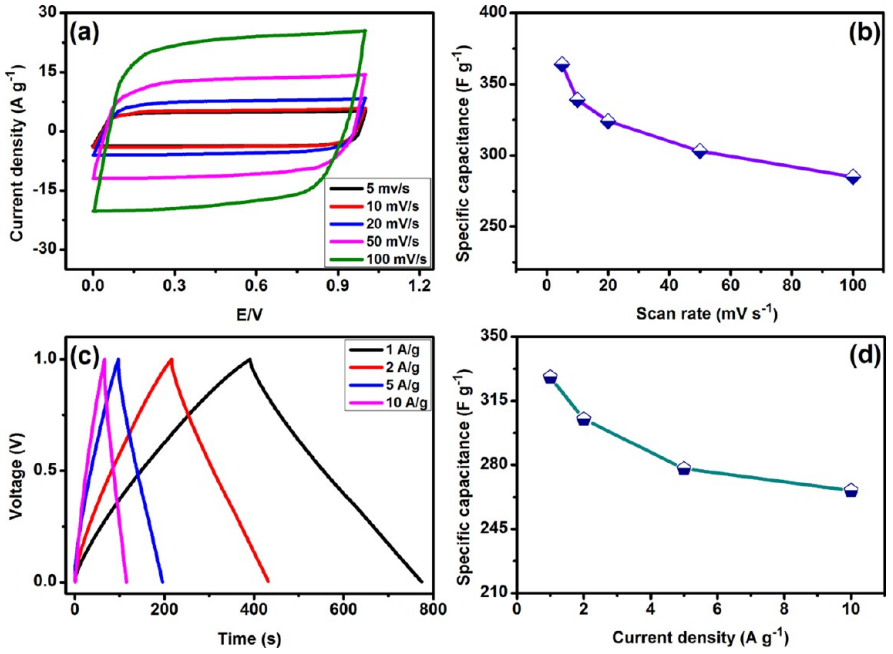

Figure 5. Electrochemical performance of the as-prepared asymmetric supercapacitor: (a) cyclic voltammograms with different scan rates; (b) variation of specific capacitance at different scan rates; (c) charge/discharge profiles at different current densities; and (d) effect of current density on specific capacitance.

des (Table 2).[15,45,48−50] The results clearly show that these hybrid materials exhibit outstanding capacitive performance, both volumetrically and gravimetrically.

Soft self-assembly of two electric double layer capacitive (EDLC) materials along with a pseudocapacitive material in a ternary composition developed the 3D architecture immensely porous as well as highly conductive, and the synergistic behavior of both materials is a possible explanation for the phenomena described in our work. All these properties allow for enhanced penetration of the electrolyte ions throughout the entire surface of electrodes, which is observed in the shape of the CV curve at high scan rates (Figure S10). The XRD analysis (Figure S6) provides evidence that the natural assembly of MWCNTs on graphene sheets and further $\pi-\pi$ interaction with PEDOT:PSS result in an increased spacing between the successive graphene layers. On their own, such graphene sheets would otherwise agglomerate, leaving insufficient space for electrolyte penetration and resulting in poor capacitance (Figure S10). The MWCNTs and the PEDOT:PSS act as highly conducting pathways for electron movement, but more importantly, MWCNTs inhibit the restacking of the graphene sheets, increase the effective surface area for enormous charge storage, and open an incredibly large number of ion exchange channels (Figure 3) which are delicately interacted with highly conductive PEDOT:PSS performing as a superfast ionic network (evidenced by conductivity analysis) during the energy storage application. It has been recently shown in a theoretical study that the addition of nanotubes with a radius smaller than 20 nm improves the electrochemical driving force for electron transfer, resulting in an increase in the double layer capacitance.[51] CNTs of such size are potentially also responsible for the altered kinetics of the modified electrodes, which is most pronounced in the cases where the tubes are not entangled or bundled, such as in our case. Moreover the naturally engineered pseudocapacitive PEDOT:PSS layer significantly boosted the charge storage and transport ability of the interlayer ionic channels created from rGO and MWCNTs in the rGCNTPP 3D architectures.[52] As such, the observed enhancement shown in our work is directly related to not only how the addition of the MWCNTs and PEDOT:PSS functionalization affect the spacing of the graphene layers, but also the way that they are respectively dispersed throughout the structure. The $\pi-\pi$ interaction between these components and the graphene surface, maximize the interaction of the highly

DOI: 10.1021/acscentsci.5b00189
ACS Cent. Sci. 2015, 1, 206−216

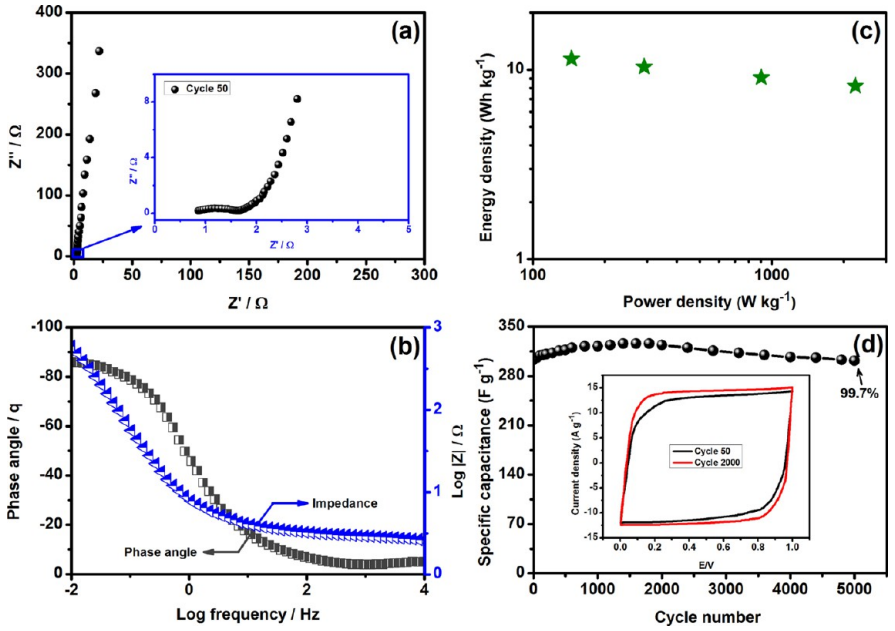

Figure 6. Electrochemical performance of the supercapacitor device: (a) Nyquist plot of the asymmetric supercapacitor, with the inset showing an enlargement of the indicated region; (b) Bode plot suggesting maximum phase angle; (c) Ragone plot showing the relationship between energy density and power density; and (d) cycle life study over 5000 cycles at 50 mV s^{-1}, with the inset showing cyclic voltammograms from cycles 50 and 2000.

conductive three-dimensional network to electrolytes and have potential contribution to the fast surface redox reactions due to the small size of electrolyte ions compared to the interlayer spacing between neighboring layers (Figure 4). These factors result in the overall synergistic effect towards enhancing the conductivity and capacitance of the final composite system. Such capacitive performance in conjunction with their excellent electrical and mechanical properties makes these architectures ideal candidates for applications in wearable energy conversion and storage, as they satisfy all the requirements for such systems, allowing the integration of graphene in supercapacitor devices.[13]

Performance of the Asymmetric Supercapacitor. To evaluate the practical nature of the rGCNTPP hybrid composites, rGCNTPP 10 was used as cathode in an asymmetric supercapacitor device (ASC) with activated carbon (AC) as the anode material (Figure 4).

A detailed overview of the CV behavior of the assembled device is presented in Figure 5a. The almost rectangular cyclic voltammograms demonstrate excellent electrical double layer capacitance (EDLC) performance and low resistivity, at both high and low scan rates. In addition to the presence of interconnected 3D networks observed in the cross-sectional FE-SEM images and the successful prevention of intersheet restacking, it should be noted that the highly charged surface profile of each individual layer serves to attract ions into the interface, causing surface charge screening and leading to the formation of an electrical double layer. Moreover, the hydrated ionic radius of SO_4^{2-} and H_3O^+ is reported to be 400 and 280 pm, respectively, which is less than the interlayer *d*-spacing here (300 to 650 pm).[11]

The maximum specific capacitance of 364 F g^{-1} was obtained at 5 mV s^{-1}, while even at the much higher scan rate of 100 mV s^{-1}, the hybrid electrode continued to provide a capacitance as high as 285 F g^{-1}, further demonstrating the easy access of ions to the whole architecture (Figure 5a,b). The minimal decrease in capacitance at higher scan rates, with retention of the rectangular CV, demonstrates the satisfactory charge transportation capability of the as-prepared layered composite in the ASC device. Galvanostatic charge/discharge (CD) cycling at different current densities was also employed to reveal the exact electrochemical capacitive performance of the supercapacitor device, as shown in Figure 5c and Figure S11. Exhibiting the same trend observed with the CV results, the differences between capacitance values observed at low and high current densities were subtle, with the hybrid material showing a capacitance value of 328 F g^{-1} at 1 A g^{-1}, while delivering an outstanding capacitance of 266 F g^{-1} at 10 A g^{-1} Figure 5c,d). Moreover, the deviation from a triangular shape was minor, indicating a negligible *IR* drop even at high current densities (Figure S12). The overall results confirm the successful formation of an efficient hybrid 3D architecture, simultaneously having both an EDL and a pseudocapacitive nature, with the fast ion transport implying the high rate capability of the as-prepared rGCNTPP 10 and low equivalent series resistance.

Electrochemical impedance spectroscopy (EIS) was conducted within the frequency range of 10 kHz to 10 mHz to map the electronic conductivity during the redox process. The Nyquist plot after 50 cycles in Figure 6a shows a very small semicircle in the high frequency region, indicating low charge transfer resistance (R_{ct}) of 0.78 Ω, while a near vertical line in the low frequency region demonstrates very good access to the electrolyte and a highly porous conductive network for the electrolyte ions to smoothly explore the whole electrode surface. The Bode plot in Figure 6b was also plotted from the Nyquist information to determine the phase angle of −86°, which is very close to −90° for an ideal supercapacitor with outstanding conductivity. The lower resistivity and superior conductivity of the chemically treated, interconnected, layered composite are also demonstrated by the high conductivity of 38700 ± 7987 S m^{-1} of the flexible rGCNTPP 10 composite film, which is much higher than those of the individual

DOI: 10.1021/acscentsci.5b00189
ACS Cent. Sci. 2015, 1, 206−216

components taken separately and of similar reported flexible composites (Table S1). By considering the total capacitance (C_T) of the assembled device, the asymmetric supercapacitor showed a promising energy density of 11.4 Wh kg^{-1} (at 1 A g^{-1}) and maximum power density of 2235 W kg^{-1} (at 10 A g^{-1}) (Figure 6c and Table S7). To highlight the outstanding consistency of the electrochemical performance of the rGCNTPP 10 3D architecture, the ASC device was tested for 5000 cycles at 50 mV s^{-1}. The electrodes showed no measurable capacitance loss, even after 5000 cycles, with capacitance retention of over 99.7% (Figure 6d).

METHODS

Materials. Liquid crystalline graphene oxide was prepared by following our previously reported method.[7,22,25,29] Carbon nanotube (CNT, Sigma, multiwalled, diameter between 6 and 13 nm) powder was functionalized and purified, employing concentrated HNO_3 for 6 h to add carboxylic groups.[7,9,28] Redispersible PEDOT:PSS pellets (Orgacon DRY, produced by Agfa), vitamin C, ethanol, poly(vinylidene difluoride) (PVDF), and activated carbon (AC) were purchased from Sigma-Aldrich and used as supplied.

Fabrication of Self-Assembled rGO-MWCNT-PEDOT:PSS Flexible Composite. To prepare a flexible reduced graphene oxide (rGO)-MWCNT-PEDOT:PSS film, homogeneous dispersions of MWCNTs and PEDOT:PSS were prepared via a simple amphiphilic self-assembly process.[7,9,29] A given amount of functionalized MWCNTs were sonicated for 1 h using conventional bath sonication, followed by 1 h sonication in an ultrasonicator (Sonics, VC505) with maximum amplitude of 30%, forming a stable homogeneous aqueous dispersion. 50 mg of liquid crystal (LC) graphene oxide (GO) dispersion (5 mg mL^{-1}) was added and vigorously stirred for 24 h to disperse the CNTs homogeneously on the surfaces of the GO sheets. The size distribution and structural composition of MWCNTs after acidification with highly concentrated acid (2.6 M HNO_3) at reflux condition and further sonication prior to attach with the GO did not change significantly, and the diameter and length of the functionalized MWCNTs remained similar to the purchased one as reported in our previous study.[7,9,28]

Redispersible PEDOT:PSS was dissolved in the GO-MWCNT composite dispersion at a weight ratio of 1:1 with respect to GO for further fabrication of PEDOT:PSS with MWCNTs. The homogeneous dispersion was incubated at 40 °C for 24 h to ensure the $\pi-\pi$ interaction of the polymer chains on the GO surfaces. The incubated dispersion was centrifuged and the excess PEDOT:PSS decanted to obtain MWCNT-PEDOT:PSS to interact with the GO sheets as a liquid crystalline dispersion. Flexible GO-MWCNT-PEDOT:PSS (GCNTPP) composite films were then prepared by casting the hybrid dispersion (5 mg mL^{-1}) on a Teflon mold. Reduction of the oxygen functional groups on the GO sheets was performed by treating the flexible film with 0.1 M vitamin C solution at 80 °C for 8 h, and the sample was then washed with ethanol and dried for 12 h at 40 °C, forming the reduced rGO-MWCNT-PEDOT:PSS (rGCNTPP). Varying amounts of MWCNTs (5, 10, and 15 wt %) were used with 50 mg of LC GO to prepare three different composites, denoted as rGCNTPP 5, 10, and 15, respectively. The as-prepared rGCNTPP composites were cut into 1.5 cm × 1 cm size to use directly as free-standing working electrodes for testing in a three-electrode system of which 1 cm × 1 cm area of the free-standing rGCNTPP electrodes was dipped in electrolyte solution during the electrochemical analysis. The average mass of the rGCNTPP electrodes used in the three-electrode system was around 0.93 to 1.0 mg cm^{-2}. To assemble the asymmetric supercapacitor device, rGCNTPP10 composite paper was cut into 1.5 cm^2 round shape (mass ≈ 2 mg) to use directly as cathode. Activated carbon (AC) and PVDF were mixed in a mass ratio of 75:25 and spread on round stainless steel substrates (1.5 cm^2) to prepare anodes for the supercapacitor devices. The mass of the active material (AC + PVDF) in an anode was ≈1 mg.

Materials and Electrochemical Characterization. The structural morphology of the as-prepared samples was studied by high-resolution transmission electron microscopy (HRTEM-JEOL F300) and field emission scanning electron microscopy (FE-SEM) (JEOL JSM-7500FA). Energy-dispersive X-ray spectroscopy (EDS) analysis and elemental mapping were conducted with an X-Flash 4010 10 mm^2, 127 eV SDD energy dispersive X-ray detector (Bruker, Billerica, MA, USA), with a working distance of 10 mm, accelerating voltage of 20 kV, and a spot size of 13. X-ray diffraction (XRD; GBC MMA) employing Cu Kα radiation (λ = 1.5406 Å, with operation at 40 keV and a cathode current of 20 mA) was also conducted. X-ray photoelectron spectroscopy (XPS) was conducted on a PHOIBOS 100 hemispherical analyzer with pass energy of 26.00 eV, 45° takeoff angle, and a beam size of 100 mm. Fourier transform infrared (FT-IR) and ultraviolet−visible (UV−vis) spectra were obtained using an AIM-8800 (Shimadzu, Japan) with the KBr pellet technique and a Shimadzu UV-3600, respectively. Thermogravimetric analysis (TGA) was conducted with a Mettler Toledo TGA/DSC1 under nitrogen atmosphere. The liquid crystalline nature of the LC GO and LC GO-MWCNT-PEDOT:PSS dispersions was examined by polarized optical microscopy (POM, Leica CTR 6000). The specific surface area of the as-prepared composite films was determined by the Brunauer−Emmett−Teller (BET) method using a Nova 1000 gas sorption instrument. The rGCNTPP composites were cut to a size of 20 × 10 mm, dipped in 1 M H_2SO_4 for 1 h at room temperature, and dried for 4 h at 50 °C, prior to being examined with the linear four-point-probe head of a JANDEL four-point-probe resistivity system (model RM3) to measure the surface conductivity at room temperature and 20 nA current. Sulfuric acid treatment at room temperature was only applied to the samples used for conductivity measurement to experience a similar conductivity effect during the electrochemical analysis (1 M H_2SO_4 used as electrolyte) of the composites. Electrochemical analysis was performed at standard temperature and pressure (STP) on a VMP3 Bio-Logic electrochemical workstation with a three-electrode configuration in a beaker-type cell. An electrolyte solution of 1 M H_2SO_4, an Ag|AgCl reference electrode, and a platinum foil counter electrode were used within the potential range of 0 to 0.9 V. An aqueous asymmetric supercapacitor (ASC) was assembled in an ECC-Std electrochemical test cell (EL-cell) with similar electrolyte and a glass fiber separator.

CONCLUSIONS

In summary, self-assembled, flexible, and mechanically robust ternary architectures for rGO-MWCNT-CP composites were fabricated, employing a novel yet facile soft self-assembly fabrication route. The approach is readily scalable and can be used to produce unlimited lengths of multifunctional flexible 3D architectures. It was demonstrated that the as-produced

DOI: 10.1021/acscentsci.5b00189
ACS Cent. Sci. 2015, 1, 206−216

architectures exhibited the attributes required of a high performing supercapacitor electrode material (761 F cm^{-3} at 5 mV s^{-1}) for integration into wearable energy conversion and storage devices, such as flexibility, light weight, intrinsically superior electrical conductivity (38700 ± 7987 S m^{-1}), interlayer spacing comparable to that of the hydrated ions present in the electrolyte, and the successful combination of a pseudocapacitive element with excellent cyclability and high rate performance. These factors, combined with the high structural integrity of the architectures, as evidenced by their high toughness (~7.3 MJ m^{-3}), make this approach a viable, innovative framework for designing next-generation, cost-effective multifunctional supercapacitor materials. By mimicking the dynamic and functional versatility of nature, the soft self-assembly of MWCNTs and PEDOT:PSS increases the potential use of such materials in energy storage applications, providing a cost-effective strategy to fabricate mechanically stable rGO-MWCNT-CP composites.

■ ASSOCIATED CONTENT

Supporting Information

The following file is available free of charge on the ACS Publications website at DOI: 10.1021/acscentsci.5b00189.

Details of the preparation and characterization of LC GO, analysis of the rGCNTPP composites, and details and discussion on capacitive performance of individual free-standing ternary composite electrodes in three-electrode system (PDF)

■ AUTHOR INFORMATION

Corresponding Author

*E-mail: konstan@uow.edu.au.

Notes

The authors declare no competing financial interest.

■ ACKNOWLEDGMENTS

The authors are grateful for their financial support from the Commonwealth of Australia, the Automotive CRC 2020, and the Australian Research Council (ARC) through a Linkage Infrastructure, Equipment and Facilities (LIEF) grant (LE130100051), and to the Institute for Superconducting and Electronic Materials (ISEM) for use of its infrastructure as part of its in-kind support.

■ REFERENCES

(1) Baughman, R. H.; Zakhidov, A. A.; de Heer, W. A. Carbon Nanotubes—the Route Toward Applications. *Science* **2002**, *297*, 787–792.

(2) De Volder, M. F. L.; Tawfick, S. H.; Baughman, R. H.; Hart, A. J. Carbon Nanotubes: Present and Future Commercial Applications. *Science* **2013**, *339*, 535–539.

(3) Geim, A. K.; Novoselov, K. S. The rise of graphene. *Nat. Mater.* **2007**, *6*, 183–191.

(4) Chung, C.; Kim, Y.-K.; Shin, D.; Ryoo, S.-R.; Hong, B. H.; Min, D.-H. Biomedical Applications of Graphene and Graphene Oxide. *Acc. Chem. Res.* **2013**, *46*, 2211–2224.

(5) Kwon, C. H.; Lee, S.-H.; Choi, Y.-B.; Lee, J. A.; Kim, S. H.; Kim, H.-H.; Spinks, G. M.; Wallace, G. G.; Lima, M. D.; Kozlov, M. E.; Baughman, R. H.; Kim, S. J. High-power biofuel cell textiles from woven biscrolled carbon nanotube yarns. *Nat. Commun.* **2014**, DOI: 10.1038/ncomms4928.

(6) Simon, P.; Gogotsi, Y. Materials for electrochemical capacitors. *Nat. Mater.* **2008**, *7*, 845–854.

(7) Aboutalebi, S. H.; Chidembo, A. T.; Salari, M.; Konstantinov, K.; Wexler, D.; Liu, H. K.; Dou, S. X. Comparison of GO, GO/MWCNTs composite and MWCNTs as potential electrode materials for supercapacitors. *Energy Environ. Sci.* **2011**, *4*, 1855–1865.

(8) Yang, X.; Zhu, J.; Qiu, L.; Li, D. Bioinspired Effective Prevention of Restacking in Multilayered Graphene Films: Towards the Next Generation of High-Performance Supercapacitors. *Adv. Mater.* **2011**, *23*, 2833–2838.

(9) Aboutalebi, S. H.; Aminorroaya-Yamini, S.; Nevirkovets, I.; Konstantinov, K.; Liu, H. K. Enhanced Hydrogen Storage in Graphene Oxide-MWCNTs Composite at Room Temperature. *Adv. Energy Mater.* **2012**, *2*, 1439–1446.

(10) Yang, X.; Cheng, C.; Wang, Y.; Qiu, L.; Li, D. Liquid-Mediated Dense Integration of Graphene Materials for Compact Capacitive Energy Storage. *Science* **2013**, *341*, 534–537.

(11) Aboutalebi, S. H.; Jalili, R.; Esrafilzadeh, D.; Salari, M.; Gholamvand, Z.; Aminorroaya Yamini, S.; Konstantinov, K.; Shepherd, R. L.; Chen, J.; Moulton, S. E.; Innis, P. C.; Minett, A. I.; Razal, J. M.; Wallace, G. G. High-Performance Multifunctional Graphene Yarns: Toward Wearable All-Carbon Energy Storage Textiles. *ACS Nano* **2014**, *8*, 2456–2466.

(12) Tang, C.; Zhang, Q.; Zhao, M.-Q.; Huang, J.-Q.; Cheng, X.-B.; Tian, G.-L.; Peng, H.-J.; Wei, F. Nitrogen-Doped Aligned Carbon Nanotube/Graphene Sandwiches: Facile Catalytic Growth on Bifunctional Natural Catalysts and Their Applications as Scaffolds for High-Rate Lithium-Sulfur Batteries. *Adv. Mater.* **2014**, *26*, 6100–6105.

(13) Bonaccorso, F.; Colombo, L.; Yu, G.; Stoller, M.; Tozzini, V.; Ferrari, A. C.; Ruoff, R. S.; Pellegrini, V. Graphene, related two-dimensional crystals, and hybrid systems for energy conversion and storage. *Science* **2015**, DOI: 10.1126/science.1246501.

(14) Jost, K.; Stenger, D.; Perez, C. R.; McDonough, J. K.; Lian, K.; Gogotsi, Y.; Dion, G. Knitted and screen printed carbon-fiber supercapacitors for applications in wearable electronics. *Energy Environ. Sci.* **2013**, *6*, 2698–2705.

(15) Raccichini, R.; Varzi, A.; Passerini, S.; Scrosati, B. The role of graphene for electrochemical energy storage. *Nat. Mater.* **2014**, DOI: 10.1038/nmat4170.

(16) Wu, Z.-S.; Parvez, K.; Winter, A.; Vieker, H.; Liu, X.; Han, S.; Turchanin, A.; Feng, X.; Müllen, K. Layer-by-Layer Assembled Heteroatom-Doped Graphene Films with Ultrahigh Volumetric Capacitance and Rate Capability for Micro-Supercapacitors. *Adv. Mater.* **2014**, *26*, 4552–4558.

(17) Bunch, J. S.; van der Zande, A. M.; Verbridge, S. S.; Frank, I. W.; Tanenbaum, D. M.; Parpia, J. M.; Craighead, H. G.; McEuen, P. L. Electromechanical Resonators from Graphene Sheets. *Science* **2007**, *315*, 490–493.

(18) Avouris, P.; Chen, Z.; Perebeinos, V. Carbon-based electronics. *Nat. Nano* **2007**, *2*, 605–615.

(19) Chen, Z.; Ren, W.; Gao, L.; Liu, B.; Pei, S.; Cheng, H.-M. Three-dimensional flexible and conductive interconnected graphene networks grown by chemical vapour deposition. *Nat. Mater.* **2011**, *10*, 424–428.

(20) Kyrylyuk, A. V.; Hermant, M. C.; Schilling, T.; Klumperman, B.; Koning, C. E.; van der Schoot, P. Controlling electrical percolation in multicomponent carbon nanotube dispersions. *Nat. Nano* **2011**, *6*, 364–369.

(21) Yu, D.; Goh, K.; Wang, H.; Wei, L.; Jiang, W.; Zhang, Q.; Dai, L.; Chen, Y. Scalable synthesis of hierarchically structured carbon nanotube-graphene fibres for capacitive energy storage. *Nat. Nano* **2014**, *9*, 555–562.

(22) Jalili, R.; Aboutalebi, S. H.; Esrafilzadeh, D.; Konstantinov, K.; Moulton, S. E.; Razal, J. M.; Wallace, G. G. Organic Solvent-Based Graphene Oxide Liquid Crystals: A Facile Route toward the Next Generation of Self-Assembled Layer-by-Layer Multifunctional 3D Architectures. *ACS Nano* **2013**, *7*, 3981–3990.

(23) Nardecchia, S.; Carriazo, D.; Ferrer, M. L.; Gutierrez, M. C.; del Monte, F. Three dimensional macroporous architectures and aerogels built of carbon nanotubes and/or graphene: synthesis and applications. *Chem. Soc. Rev.* **2013**, *42*, 794–830.

(24) Qiu, L.; Yang, X.; Gou, X.; Yang, W.; Ma, Z.-F.; Wallace, G. G.; Li, D. Dispersing Carbon Nanotubes with Graphene Oxide in Water and Synergistic Effects between Graphene Derivatives. *Chem.—Eur. J.* **2010**, *16*, 10653−10658.
(25) Aboutalebi, S. H.; Gudarzi, M. M.; Zheng, Q. B.; Kim, J.-K. Spontaneous Formation of Liquid Crystals in Ultralarge Graphene Oxide Dispersions. *Adv. Funct. Mater.* **2011**, *21*, 2978−2988.
(26) Chidembo, A.; Aboutalebi, S. H.; Konstantinov, K.; Salari, M.; Winton, B.; Yamini, S. A.; Nevirkovets, I. P.; Liu, H. K. Globular reduced graphene oxide-metal oxide structures for energy storage applications. *Energy Environ. Sci.* **2012**, *5*, 5236−5240.
(27) Chidembo, A. T.; Aboutalebi, S. H.; Konstantinov, K.; Jafta, C. J.; Liu, H. K.; Ozoemena, K. I. In situ engineering of urchin-like reduced graphene oxide-Mn2O3-Mn3O4 nanostructures for supercapacitors. *RSC Adv.* **2014**, *4*, 886−892.
(28) Chidembo, A. T.; Aboutalebi, S. H.; Konstantinov, K.; Wexler, D.; Liu, H. K.; Dou, S. X. Liquid Crystalline Dispersions of Graphene-Oxide-Based Hybrids: A Practical Approach towards the Next Generation of 3D Isotropic Architectures for Energy Storage Applications. *Part. Part. Syst. Charact.* **2014**, *31*, 465−473.
(29) Islam, M.; Chidembo, A.; Aboutalebi, H.; Cardillo, D.; Liu, H. K.; Konstantinov, K.; Dou, S. X. Liquid crystalline graphene oxide/PEDOT:PSS self-assembled 3D architecture for binder-free supercapacitor electrodes. *Front. Energy Res.* **2014**, DOI: 10.3389/fenrg.2014.00031.
(30) Bisoyi, H. K.; Kumar, S. Liquid-crystal nanoscience: an emerging avenue of soft self-assembly. *Chem. Soc. Rev.* **2011**, *40*, 306−319.
(31) Graydon, O. Liquid crystals: Self-assembled fibres. *Nat. Photonics* **2014**, *8*, 84−84.
(32) Tschierske, C. Development of Structural Complexity by Liquid-Crystal Self-assembly. *Angew. Chem., Int. Ed.* **2013**, *52*, 8828−8878.
(33) Moreno-Razo, J. A.; Sambriski, E. J.; Abbott, N. L.; Hernandez-Ortiz, J. P.; de Pablo, J. J. Liquid-crystal-mediated self-assembly at nanodroplet interfaces. *Nature* **2012**, *485*, 86−89.
(34) Lee, J. A.; Shin, M. K.; Kim, S. H.; Cho, H. U.; Spinks, G. M.; Wallace, G. G.; Lima, M. D.; Lepró, X.; Kozlov, M. E.; Baughman, R. H.; Kim, S. J. Ultrafast charge and discharge biscrolled yarn supercapacitors for textiles and microdevices. *Nat. Commun.* **2013**, DOI: 10.1038/ncomms2970.
(35) Xia, Y.; Sun, K.; Ouyang, J. Solution-Processed Metallic Conducting Polymer Films as Transparent Electrode of Optoelectronic Devices. *Adv. Mater.* **2012**, *24*, 2436−2440.
(36) Xu, Z.; Gao, C. Graphene chiral liquid crystals and macroscopic assembled fibres. *Nat. Commun.* **2011**, *2*, 571.
(37) Jalili, R.; Aboutalebi, S. H.; Esrafilzadeh, D.; Shepherd, R. L.; Chen, J.; Aminorroaya-Yamini, S.; Konstantinov, K.; Minett, A. I.; Razal, J. M.; Wallace, G. G. Scalable One-Step Wet-Spinning of Graphene Fibers and Yarns from Liquid Crystalline Dispersions of Graphene Oxide: Towards Multifunctional Textiles. *Adv. Funct. Mater.* **2013**, *23*, 5345−5354.
(38) Xu, Z.; Sun, H.; Zhao, X.; Gao, C. Ultrastrong Fibers Assembled from Giant Graphene Oxide Sheets. *Adv. Mater.* **2013**, *25*, 188−193.
(39) Sweetman, L. J.; Nghiem, L.; Chironi, I.; Triani, G.; in het Panhuis, M.; Ralph, S. F. Synthesis, properties and water permeability of SWNT buckypapers. *J. Mater. Chem.* **2012**, *22*, 13800−13810.
(40) Ballard, D. G. H.; Rideal, G. R. Flexible inorganic films and coatings. *J. Mater. Sci.* **1983**, *18*, 545−561.
(41) Reynolds, R. A., III; Greinke, R. A. Influence of expansion volume of intercalated graphite on tensile properties of flexible graphite. *Carbon* **2001**, *39*, 479−481.
(42) Leng, Y.; Gu, J.; Cao, W.; Zhang, T.-Y. Influences of density and flake size on the mechanical properties of flexible graphite. *Carbon* **1998**, *36*, 875−881.
(43) Olek, M.; Ostrander, J.; Jurga, S.; Möhwald, H.; Kotov, N.; Kempa, K.; Giersig, M. Layer-by-Layer Assembled Composites from Multiwall Carbon Nanotubes with Different Morphologies. *Nano Lett.* **2004**, *4*, 1889−1895.
(44) Heywang, G.; Jonas, F. Poly(alkylenedioxythiophene)s—new, very stable conducting polymers. *Adv. Mater.* **1992**, *4*, 116−118.
(45) Lis, D.; Backus, E. H. G.; Hunger, J.; Parekh, S. H.; Bonn, M. Liquid flow along a solid surface reversibly alters interfacial chemistry. *Science* **2014**, *344*, 1138−1142.
(46) Wernet, P.; Nordlund, D.; Bergmann, U.; Cavalleri, M.; Odelius, M.; Ogasawara, H.; Näslund, L. Å.; Hirsch, T. K.; Ojamäe, L.; Glatzel, P.; Pettersson, L. G. M.; Nilsson, A. The Structure of the First Coordination Shell in Liquid Water. *Science* **2004**, *304*, 995−999.
(47) Chen, H.; Müller, M. B.; Gilmore, K. J.; Wallace, G. G.; Li, D. Mechanically Strong, Electrically Conductive, and Biocompatible Graphene Paper. *Adv. Mater.* **2008**, *20*, 3557−3561.
(48) Ghidiu, M.; Lukatskaya, M. R.; Zhao, M.-Q.; Gogotsi, Y.; Barsoum, M. W. Conductive two-dimensional titanium carbide 'clay' with high volumetric capacitance. *Nature* **2014**, *516*, 78−81.
(49) Murali, S.; Quarles, N.; Zhang, L. L.; Potts, J. R.; Tan, Z.; Lu, Y.; Zhu, Y.; Ruoff, R. S. Volumetric capacitance of compressed activated microwave-expanded graphite oxide (a-MEGO) electrodes. *Nano Energy* **2013**, *2*, 764−768.
(50) Yoon, Y.; Lee, K.; Kwon, S.; Seo, S.; Yoo, H.; Kim, S.; Shin, Y.; Park, Y.; Kim, D.; Choi, J.-Y.; Lee, H. Vertical Alignments of Graphene Sheets Spatially and Densely Piled for Fast Ion Diffusion in Compact Supercapacitors. *ACS Nano* **2014**, *8*, 4580−4590.
(51) Henstridge, M. C.; Dickinson, E. J. F.; Compton, R. G. On the estimation of the diffuse double layer of carbon nanotubes using classical theory: Curvature effects on the Gouy−Chapman limit. *Chem. Phys. Lett.* **2010**, *485*, 167−170.
(52) D'Arcy, J. M.; El-Kady, M. F.; Khine, P. P.; Zhang, L.; Lee, S. H.; Davis, N. R.; Liu, D. S.; Yeung, M. T.; Kim, S. Y.; Turner, C. L.; Lech, A. T.; Hammond, P. T.; Kaner, R. B. Vapor-Phase Polymerization of Nanofibrillar Poly(3,4-ethylenedioxythiophene) for Supercapacitors. *ACS Nano* **2014**, *8*, 1500−1510.
(53) Cheng, Q.; Tang, J.; Shinya, N.; Qin, L.-C. Polyaniline modified graphene and carbon nanotube composite electrode for asymmetric supercapacitors of high energy density. *J. Power Sources* **2013**, *241*, 423−428.
(54) Huang, L.; Li, C.; Shi, G. High-performance and flexible electrochemical capacitors based on graphene/polymer composite films. *J. Mater. Chem. A* **2014**, *2*, 968−974.
(55) Zhou, Y.; Lachman, N.; Ghaffari, M.; Xu, H.; Bhattacharya, D.; Fattahi, P.; Abidian, M. R.; Wu, S.; Gleason, K. K.; Wardle, B. L.; Zhang, Q. M. A high performance hybrid asymmetric supercapacitor via nano-scale morphology control of graphene, conducting polymer, and carbon nanotube electrodes. *J. Mater. Chem. A* **2014**, *2*, 9964−9969.
(56) Fan, L.-Q.; Liu, G.-J.; Wu, J.-H.; Liu, L.; Lin, J.-M.; Wei, Y.-L. Asymmetric supercapacitor based on graphene oxide/polypyrrole composite and activated carbon electrodes. *Electrochim. Acta* **2014**, *137*, 26−33.
(57) Shen, J.; Yang, C.; Li, X.; Wang, G. High-Performance Asymmetric Supercapacitor Based on Nanoarchitectured Polyaniline/Graphene/Carbon Nanotube and Activated Graphene Electrodes. *ACS Appl. Mater. Interfaces* **2013**, *5*, 8467−8476.
(58) Yu, X.; Park, H. S. Sulfur-incorporated, porous graphene films for high performance flexible electrochemical capacitors. *Carbon* **2014**, *77*, 59−65.
(59) Li, P.; Shi, E.; Yang, Y.; Shang, Y.; Peng, Q.; Wu, S.; Wei, J.; Wang, K.; Zhu, H.; Yuan, Q.; Cao, A.; Wu, D. Carbon nanotube-polypyrrole core-shell sponge and its application as highly compressible supercapacitor electrode. *Nano Res.* **2014**, *7*, 209−218.
(60) Lin, H.; Li, L.; Ren, J.; Cai, Z.; Qiu, L.; Yang, Z.; Peng, H. Conducting polymer composite film incorporated with aligned carbon nanotubes for transparent, flexible and efficient supercapacitor. *Sci. Rep.* **2013**, DOI: 10.1038/srep01353.
(61) Meng, Y.; Wang, K.; Zhang, Y.; Wei, Z. Hierarchical Porous Graphene/Polyaniline Composite Film with Superior Rate Performance for Flexible Supercapacitors. *Adv. Mater.* **2013**, *25*, 6985−6990.
(62) Liu, F.; Wang, S.; Han, G.; Liu, R.; Chang, Y.; Xiao, Y. Multiwalled carbon nanotubes/polypyrrole/graphene/nonwoven fab-

DOI: 10.1021/acscentsci.5b00189
ACS Cent. Sci. 2015, 1, 206−216

ric composites used as electrodes of electrochemical capacitor. *J. Appl. Polym. Sci.* **2014**, DOI: 10.1002/app.41023.
(63) Weng, Y.-T.; Wu, N.-L. High-performance poly(3,4-ethylenedioxythiophene):polystyrenesulfonate conducting-polymer supercapacitor containing hetero-dimensional carbon additives. *J. Power Sources* **2013**, *238*, 69−73.
(64) Zhang, J.; Zhao, X. S. Conducting Polymers Directly Coated on Reduced Graphene Oxide Sheets as High-Performance Supercapacitor Electrodes. *J. Phys. Chem. C* **2012**, *116*, 5420−5426.
(65) Sun, D.; Jin, L.; Chen, Y.; Zhang, J.-R.; Zhu, J.-J. Microwave-Assisted In Situ Synthesis of Graphene/PEDOT Hybrid and Its Application in Supercapacitors. *ChemPlusChem* **2013**, *78*, 227−234.

DOI: 10.1021/acscentsci.5b00189
ACS Cent. Sci. 2015, 1, 206−216